Thermodynamics of RNA Duplexes with Tandem Mismatches Containing a Uracil-Uracil Pair Flanked by C·G/G·C or G·C/A·U Closing Base Pairs†

Brooke N. Bourdélat-Parks and Roger M. Wartell*

School of Biology, Georgia Institute of Technology, Atlanta, Georgia 30332

Received August 19, 2005; Revised Manuscript Received October 20, 2005

ABSTRACT: The thermodynamics governing the denaturation of RNA duplexes containing 8 bp and a central tandem mismatch or 10 bp were evaluated using UV absorbance melting curves. Each of the eight tandem mismatches that were examined had one U-U pair adjacent to another noncanonical base pair. They were examined in two different RNA duplex environments, one with the tandem mismatch closed by G·C base pairs and the other with G·C and A·U closing base pairs. The free energy increments (ΔG°_{loop}) of the 2 × 2 loops were positive, and showed relatively small differences between the two closing base pair environments. Assuming temperature-independent enthalpy changes for the transitions, ΔG°_{loop} for the 2 × 2 loops varied from 0.9 to 1.9 kcal/mol in 1 M Na^+ at 37 °C. Most values were within 0.8 kcal/mol of previously estimated values; however, a few sequences differed by 1.2−2.0 kcal/mol. Single strands employed to form the RNA duplexes exhibited small noncooperative absorbance increases with temperature or transitions indicative of partial self-complementary duplexes. One strand formed a partial self-complementary duplex that was more stable than the tandem mismatch duplexes it formed. Transitions of the RNA duplexes were analyzed using equations that included the coupled equilibrium of self-complementary duplex and non-self-complementary duplex denaturation. The average heat capacity change (ΔC_p) associated with the transitions of two RNA duplexes was estimated by plotting ΔH° and ΔS° evaluated at different strand concentrations as a function of T_m and ln T_m, respectively. The average ΔC_p was 70 ± 5 cal K^{-1} (mol of base pairs)$^{-1}$. Consideration of this heat capacity change reduced the free energy of formation at 37 °C of the 10 bp control RNA duplexes by 0.3−0.6 kcal/mol, which may increase ΔG°_{loop} values by similar amounts.

Prediction of RNA secondary structure by free energy minimization using nearest-neighbor parameters has provided insight into the structure−function relationships of RNA molecules (*1*−*5*). The method has been utilized to predict RNA structures and examine their roles in transcription and translation (*6*−*8*), to guide experiments that evaluate the presence of structural motifs in RNAs (*9*−*12*), and to aid in the design of RNA molecules (*13*, *14*). A recent evaluation of the accuracy of RNA secondary structure prediction indicates that 73% of known canonical base pairs are predicted for a database of ∼150000 nt[1] (*4*).

Thermodynamic parameters that form the basis of structure prediction algorithms are evaluated or extrapolated from studies on model RNAs containing specific sequence−structure motifs (*1*, *15*). Studies on RNAs with canonical A·U, G·C, and G·U base pairs have provided a complete set of parameters for calculation of the stability of duplex segments with Watson−Crick base pairs (*16*). Parameters have also been measured for a large number of single bulges (*17*, *18*), single-mismatch loops (*19*−*21*), and hairpin loops (*22*, *23*), as well as tandem mismatch loops (*1*, *19*, *24*−*26*), 3 × 3 loops (*27*), and asymmetric loops (*28*−*30*). Because of the enormous number of possible sequence variants in internal loops, extrapolated estimates of thermodynamic parameters are employed for most loops (*4*). Additional information about the sequence dependence of internal loop formation can be expected to improve secondary structure predictions.

Previous work has shown that tandem U-U mismatches between G·C base pairs contributes a negative free energy at 37 °C in 1 M Na^+ (*31*). The presence of a U-U mismatch within some internal loops has a stabilizing effect, and it is generally regarded as a stabilizing mismatch (*28*, *30*). In this study, we examined the stability of 16 RNA duplexes containing one tandem mismatch consisting of a U-U mismatch adjacent to another noncanonical base pair. Eight tandem mismatches were examined flanked by two closing G·C base pairs or by a G·C and A·U base pair. The free energy increments of the 2 × 2 loops were always positive, ranging from 0.9 to 1.9 kcal/mol. The values were not strongly affected by the closing base pair environments that were examined. While most tandem mismatches gave loop free energies that were within 0.8 kcal/mol of previously estimated values, the GU/UA tandem mismatch was less stable than predicted by ∼1.9 kcal/mol for both closing base pair environments. The average heat capacity change associated with two RNA transitions was estimated from plots

† This work was supported by funding from CRDF and the College of Sciences, Georgia Tech.

* To whom correspondence should be addressed. E-mail: roger.wartell@biology.gatech.edu. Phone: (404) 894-8421. Fax: (404) 894-0519.

[1] Abbreviations: nt, nucleotide; T_m, midpoint transition temperature; UV, ultraviolet.

10.1021/bi051659q CCC: $30.25
Published on Web 11/22/2005

FIGURE 1: Sequence and schematic structures of the RNA duplex molecules that were examined. The name given to each strand is on the right, and the name given to the duplex is below each structure.

of enthalpy and entropy change as a function of T_m and ln T_m. The value that is obtained [$\Delta C_p = 70 \pm 5$ cal K^{-1} (mol of base pairs)$^{-1}$] is similar to values obtained from previous studies (*32*, *33*). Consideration of this non-zero heat capacity change may increase the ΔG°_{loop} values by 0.3−0.6 kcal/mol.

MATERIALS AND METHODS

RNA Oligonucleotides. The RNA oligonucleotides used in this study were synthesized commercially (Dharmacon Inc.) and deprotected prior to purification using a HPLC system. A Dionex DNAPac PA-100 anion exchange column was employed with a sodium perchlorate gradient. The oligonucleotides were desalted using a Sep-Pak C-18 cartridge, eluted with a solution of 35% methanol, 35% acetonitrile, and 30% TEAB (50 mM), and dried. An additional desalting step was carried out for samples used at high concentrations by resuspension of samples in water and elution through a Sephadex G-10 column. Fractions containing the RNA were dried and resuspended in TE (10 mM Tris and 1 mM EDTA). All oligonucleotides produced a single band on a 16.5 cm × 20 cm denaturing 20% polyacrylamide gel. Figure 1 shows the RNA oligonucleotides employed and the RNA duplexes expected from annealing equimolar amounts of strands. Aqueous solutions were made with DEPC-treated water.

The concentration of each single-stranded oligonucleotide was determined from the 260 nm absorbance value linearly extrapolated to 25 °C from absorbance versus temperature plots between 50 and 75 °C. Oligonucleotide samples were characterized at concentrations corresponding to approximately 0.3 OD/mL. The extinction coefficient of each strand was calculated on the basis of its dinucleotide frequencies and composition (*34*, *35*).

UV Melting Experiments. UV absorbance was employed to monitor the melting transitions of the duplex RNA molecules and to characterize the temperature-dependent transitions of the single strands. To form duplexes, complementary single strands were mixed at equimolar concentrations and slowly cooled from 70 °C. Most melting curves were obtained using a 1.0 M Na^+ buffer [0.978 M NaCl, 0.01 M Na_2HPO_4 (pH 7.5), and 1 mM Na_2EDTA]. For some samples, a 0.1 M Na^+ buffer was employed [0.078 M NaCl, 0.01 M Na_2HPO_4 (pH 7.0), and 1 mM Na_2EDTA]. The concentration employed for UV melting experiments of RNA duplexes was generally between 4 and 6 μM strands. Melting curves of two RNA duplexes were obtained at six concentrations between 1 and 75 μM.

Samples were placed in 1 cm path length quartz cuvettes, and a Cary 100 spectrophotometer (Varian, Inc.) was used to measure absorbance as a function of temperature at 268 or 280 nm with a heating rate of 0.5 °C/min. The temperature was measured with a platinum resistance probe inserted into a solvent cell adjacent to the sample. Absorbance readings were taken every 0.1 °C over a range from 5 to 75 °C. Three or more melting transitions were obtained for each sample.

Calculation of Thermodynamic Parameters from the UV Denaturation Curve. Absorbance versus temperature data obtained from the denaturation or melting curves of the RNA duplexes were expressed as the fraction of total strands in the single-stranded state, θ_s, using the following equation:

$$\theta_s(T) = [A(T) - A_{pre}(T)]/[A_{post}(T) - A_{pre}(T)] \quad (1)$$

where $A(T)$ is the absorbance of the sample at temperature T and $A_{pre}(T)$ and $A_{post}(T)$ are the pre- and post-transition linear baselines of the denaturation curves, respectively. For duplexes with a T_m of <42 °C, the denaturation curves left little choice with regard to linear baselines covering 10−15 °C before and after the main transition. For the two fully base paired duplexes with higher T_m's, pretransition absorbance changes starting from ~5 °C curved slightly upward (e.g., Figure 2) and the point at which to draw the baselines were more subjective. To maintain a consistent approach, pretransition baselines were drawn over the 15 °C region just below the main transition. This approach gave results in excellent agreement with previous work (Table 1), and produced $\theta_s(T)$ curves that were fit better by eq 2. Using the lower-temperature region for the linear baseline reduced the peak of the derivative curve, and the evaluated free energies were reduced by ~0.8 kcal/mol.

Assuming the transitions from the duplex to single strands are two-state (S1·S2 $\rightleftarrows$ S1 + S2), $\theta_s(T)$ can be related to the apparent equilibrium dissociation constant K_d and total strand concentration C_t by the equation

$$\theta_s(T) = K_d[(1 + 2C_t/K_d)^{1/2} - 1]/C_t \quad (2)$$

To determine apparent ΔH° and ΔS° values, K_d was expressed in terms of these parameters and a nonlinear least-

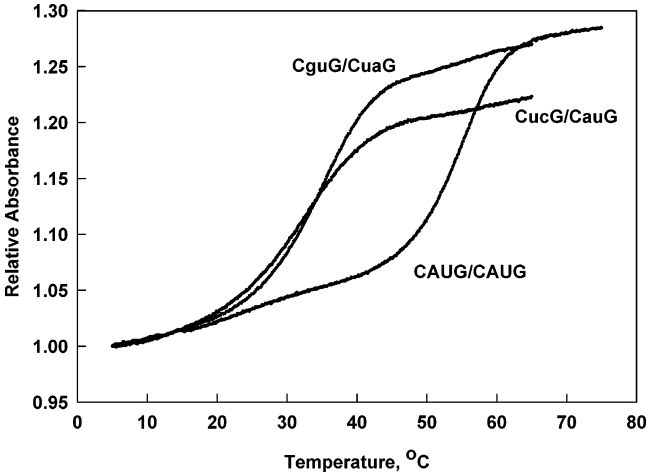

FIGURE 2: Relative absorbance vs temperature plots of three RNA duplex molecules examined in 1 M Na^+. Shown are the melting curves of CAUG/CAUG, CucG/CauG, and CguG/CuaG. Absorbance changes were monitored at 268 nm and normalized to their values at the initial temperatures that were measured. The total strand concentration for these samples was 5−6 μM.

squares regression (SigmaPlot) was employed to evaluate $\Delta H°$ and $\Delta S°$ pairs that best fit the shape of the RNA melting curves (eqs 1 and 2). The $\theta_s(T)$ data range of 0.1−0.9 was employed. Correlation coefficients (R^2) of ≥0.99 were observed for the fits to the melting curves. Reported $\Delta H°$ and $\Delta S°$ values and their standard deviations were based on three experiments.

Several single-stranded oligonucleotides exhibited absorbance−temperature profiles and concentration-dependent T_m's indicative of self-complementary duplex transitions. These transitions were analyzed in a manner similar to that described for eqs 1 and 2 with a modification to eq 2 appropriate for self-complementary duplexes (*36*). C_t in eq 2 was replaced by $4C_t$. Analysis of the transitions of the non-self-complementary RNA duplexes in which one or both strands could form a self-complementary duplex was carried out using equations that described the coupled melting equilibria (Appendix).

RESULTS

Design of Oligodeoxynucleotides. Figure 1 shows the expected structures of the 18 RNA duplex molecules examined in this study. One set of molecules (set 1) utilized pairs of single-stranded molecules with 5′ CGAGXYAGGC 3′ (top strand) and 5′ GCCUWZCUCG 3′ (bottom strand) sequences, where X-Z and Y-W represent mismatched or complementary base pairs. A·U and G·C closing base pairs surround the central 5′ XY 3′/5′ WZ 3′ base pairs. The second set of molecules (set 2) employed pairs of single-stranded oligonucleotides with 5′ CCUCXYGUGA 3′ (top strands) and 5′ UCGCWZGAGG 3′ (bottom strands) sequences. For these molecules, C·G and G·C base pairs were closing base pairs surrounding the two central paired bases. The single-strand and duplex names are given in Figure 1. Lowercase letters are employed in the duplex names to designate noncanonical base pairs.

RNA Duplex Transition Curves in 1 M Na^+. Figure 2 shows typical UV-monitored melting curves of three RNA duplexes: the fully base paired control RNA, CAUG/CAUG (curve A), and two tandem mismatch RNAs CucG/CauG (curve B) and CguG/CuaG (curve C). Absorbance changes were monitored at 268 nm and normalized to their values at the initial temperatures that were measured. Some RNA melting curves were also monitored at 280 nm. They gave similar results. Transitions were reversible for two temperature cycles. The small quasi-linear pre- and post-transition absorbance changes were typical for all duplex RNA transitions.

Absorbance−temperature measurements were carried out in 1 M Na^+ on the single-stranded oligonucleotides that formed the duplex RNAs. The single strands exhibited varying absorbance−temperature profiles. Figure 3 shows four curves representative of the behavior observed at strand concentrations of 3−5 μM. The quasi-linear increase in absorbance with temperature observed for 1TAU was observed for 1TUU, 1TGU, and 2TCU. Strand 2TUU produced a small change in absorbance from 5 to 70 °C. Low-stability cooperative transitions similar to that shown for 2TUA were observed for single strands 1TCU, 1BUA, 1BAU, 1BUC, 2TAU, and 2BUA. Their T_m's were estimated to be 8−21 °C. The transition of the 2BUC strand occurred at what was initially considered to be a surprisingly high temperature [$T_m \approx 47.7$ °C for $C_t = 4.8$ μM (Figure 3)]. The probable structure of 2BUC is described in the Discussion.

The effect of strand concentration was examined for several of the cooperative single-strand transitions (e.g., 2TUA and 2BUC). In all cases that were examined, self-complementary duplexes were indicated. Increasing the strand concentration by 7−10-fold increased T_m's by 6−9 °C. A previous study also showed that single-stranded RNAs, 8−12 nt long, frequently form stable self-complementary structures (*28*). To analyze the low-stability transitions, it was necessary to make an assumption regarding their low-temperature baselines. The baselines were assigned absorbance values at −10 °C extrapolated from the transition curves (*37*). In a few instances, the extrapolated lower baseline value was slightly adjusted to enhance the quality of the least-squares fit of the two-state transition model to the normalized melting curve. The Supporting Information lists the thermodynamic parameters evaluated from the transitions of single-stranded oligonucleotides.

Table 1 lists the thermodynamic parameters evaluated from the melting curves of the RNA duplexes with 10 bp or 8 bp and a tandem mismatch. $\Delta G°$ values at 37 °C determined for the two 10 bp RNAs were in very good agreement with values predicted from nearest neighbor parameters (*16*). The latter values are given in parentheses in Table 1. The competition of the single strands that could form self-complementary duplexes on the melting curve of the non-self-complementary duplexes was analyzed using equations describing the coupled melting equilibrium (Appendix). For most RNA duplexes, the influence of the single-stranded structures on the evaluation of parameters from the transitions of the tandem mismatch duplexes was small. The enthalpy change evaluated from a least-squares curve fit using eq 2 produced values within experimental error (1−3 kcal/mol) of the more rigorous analysis. For the tandem RNA duplexes formed with the 2BCU strand, however, analysis using the coupled melting equilibrium was essential.

Figure 4 shows the normalized melting curves of the three tandem mismatch RNAs (CauG/CucG, CcuG/CucG, and

Table 1: Thermodynamic Parameters Evaluated from RNA Transitions in 1.0 M Na^+

RNA	T_m[a] (°C)	$-\Delta H°$ (kcal/mol)	$-\Delta S°$ (eu)	$\Delta G_{37}°$ (kcal/mol)
set 1				
GAUA/UAUC	61.8 ± 0.2	100.1 ± 3.1	271.1 ± 9.5	−16.02 ± 0.18 (−16.24)[b]
GucA/UauC	40.6 ± 0.5	83.4 ± 1.3	238.5 ± 0.7	−9.41 ± 0.03
GuaA/UauC	42.8 ± 0.2	86.3 ± 2.0	245.9 ± 5.7	−10.03 ± 0.03
GauA/UuaC	41.4 ± 0.2	80.1 ± 2.0	227.6 ± 3.6	−9.54 ± 0.06
GguA/UuaC	43.8 ± 0.2	88.6 ± 4.1	252.4 ± 10.3	−10.34 ± 0.10
GcuA/UuaC	42.2 ± 0.2	81.3 ± 1.5	230.5 ± 3.0	−9.80 ± 0.03
GauA/UucC	41.5 ± 0.2	80.2 ± 1.4	227.6 ± 2.2	−9.56 ± 0.02
GcuA/UucC	42.0 ± 0.2	94.5 ± 1.3	272.5 ± 4.3	−9.97 ± 0.07
GuuA/UucC	44.4 ± 0.4	86.5 ± 4.5	245.6 ± 5.4	−10.38 ± 0.05
set 2				
CAUG/CAUG	55.0 ± 0.3	−106.5 ± 1.6	−297.05 ± 1.8	−14.32 ± 0.12 (−14.47)[b]
CucG/CauG	31.1 ± 0.3	−57.8 ± 1.0	−162.7 ± 2.7	−7.29 ± 0.03
CuaG/CauG	32.4 ± 0.2	−61.3 ± 1.1	−173.5 ± 2.5	−7.48 ± 0.07
CauG/CuaG	31.8 ± 0.3	−63.0 ± 1.5	−179.7 ± 0.2	−7.31 ± 0.08
CguG/CuaG	33.4 ± 0.3	−72.9 ± 1.4	−210.5 ± 3.4	−7.62 ± 0.02
CcuG/CuaG	33.0 ± 0.3	−65.4 ± 1.8	−186.7 ± 5.3	−7.55 ± 0.04
CauG/CucG[c]	33.0 ± 0.4	−72.4 ± 2.0	−209.8 ± 4.6	−7.34 ± 0.10
CcuG/CucG[c]	33.6 ± 0.4	−75.5 ± 1.5	−219.4 ± 5.4	−7.47 ± 0.07
CuuG/CucG[c]	34.5 ± 0.5	−73.0 ± 1.8	−210.8 ± 4.5	−7.61 ± 0.06

[a] T_m values for strand concentrations of 5−7 μM. [b] Values in parentheses are predicted using nearest neighbor free energy parameters (*16*). [c] Values obtained from the best fit of calculated transitions using eqs 12 and 13 or eq 16.

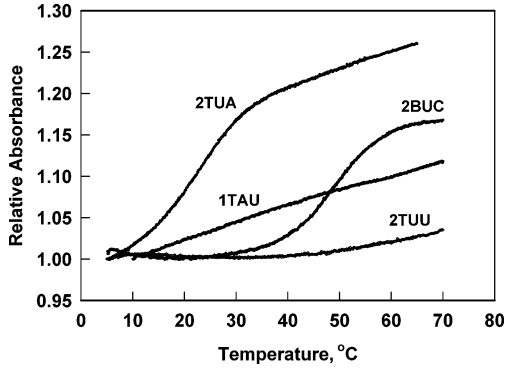

FIGURE 3: Plots of relative absorbance vs temperature for four single strands in 1 M Na^+. Each plot is labeled using the convention described in Figure 1. Strand concentrations were 3.4−5 μM.

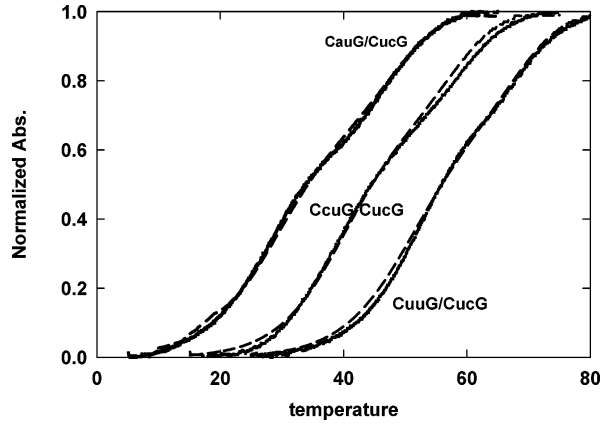

FIGURE 4: Normalized experimental (—) and calculated (− − −) melting curves of RNA duplexes CauG/CucG, CcuG/CucG, and CuuG/CucG. The curve for the CcuG/CucG duplex is shifted 10 °C higher and the curve for the CuuG/CucG duplex 20 °C higher to display the three curves without overlap. The strand concentration was 5 μM.

CuuG/CucG) formed with 2BCU and a complementary strand. Each of the curves shows a two-step transition. The second step of each transition occurred between 45.7 and 48.0 °C, corresponding to the T_m of the melting curve of 2BUC alone. The fractions of self-complementary and non-self-complementary duplexes were calculated as a function of temperature and summed appropriately to produce normalized melting curves. The algorithm employed $\Delta H°$ and $\Delta S°$ values determined from the transitions of the single strand alone, the concentration of strands in the experiment, iterative trials of $\Delta H°$, and T_m values corresponding to the unwinding of the tandem mismatch RNA. The dashed lines show best-fit theoretical curves.

Table 2: Thermodynamic Parameters for Tandem Mismatch Internal Loop Formation[a]

RNA	$-\Delta G°_{loop}$(exp) (kcal/mol)	$-\Delta G°_{loop}$(pred) (kcal/mol)	$-\Delta H°_{loop}$ (kcal/mol)	$-\Delta S°_{loop}$ (eu)
set 1				
GucA/UauC	1.9	1.1	14.7	54.0
GuaA/UauC	1.3	1.7	17.6	61.4
GauA/UuaC	1.8	1.9	11.4	43.1
GguA/UuaC	1.0	−0.7	19.9	67.9
GcuA/UuaC	1.5	1	12.6	46.0
GauA/UucC	1.8	1	11.5	43.0
GcuA/UucC	1.4	1	25.3	88.0
GuuA/UucC	0.9	1	17.8	61.1
set 2				
CucG/CauG	1.8	0.8	−1.9	0.9
CuaG/CauG	1.6	1	1.7	11.7
CauG/CuaG	1.8	1	3.4	17.9
CguG/CuaG	1.5	−0.5	13.3	48.7
CcuG/CuaG	1.5	0.3	5.8	24.9
CauG/CucG	1.8	0.8	12.8	48.0
CcuG/CucG	1.6	0.6	15.9	57.6
CuuG/CucG	1.5	0.5	13.4	49.0

[a] Experimental loop free energies were calculated using eq 3 as described in the text. Predicted loop free energies were from ref *4*. Standard deviations for experimental $\Delta G°_{loop}$ values were estimated to be ±0.20 for set 1 loops and ±0.15 for set 2 loops. $\Delta H°_{loop}$ and $\Delta S°_{loop}$ were calculated using equations analogous to eq 3a using data in Table 1 and predicted $\Delta H°_{duplex\ without\ loop}$ and $\Delta S°_{duplex\ without\ loop}$ values.

Internal Loop Free Energies of Tandem Mismatches. Table 2 lists the free energies of the tandem mismatch loops at 37 °C. The values were calculated using the equation

$$\Delta G°_{loop} = \Delta G°_{duplex\ with\ loop} - (\Delta G°_{duplex\ without\ loop} - \Delta G°_{interrupted\ base\ pair}) \quad (3a)$$

The last term of the equation, $\Delta G°_{duplex\ without\ loop} - \Delta G°_{interrupted\ base\ pair}$, subtracts the energetic contribution to the RNA molecule not involved in the loop. This term was

obtained in two ways. Method 1 calculated $\Delta G^\circ_{\text{duplex without loop}}$ for the 8 bp duplex using empirical nearest neighbor free energy parameters, and the appropriate nearest neighbor free energy term for $\Delta G^\circ_{\text{interrupted base pair}}$ (*16*). Method 2 employed the free energies ΔG°_{37} determined from the transitions of the 10 bp Watson−Crick RNA duplexes. Three nearest neighbor stacking energies were subtracted from these free energies to produce a term equivalent to the last term of eq 3a. For the CuuG/CucG example, the free energy terms using method 2 correspond to the configurations

$$\begin{matrix}5'\text{C}\,^{\text{UU}}\text{G}\\ 3'\text{G}_{\text{CU}}\,\text{C}\end{matrix} = \begin{matrix}5'\text{CCUC}\,^{\text{UU}}\text{GUGA}\\ 3'\text{GGAG}_{\text{CU}}\,\text{CGCU}\end{matrix} - \left(\begin{matrix}5'\text{CCUCAUGUGA}\\ 3'\text{GGAGUACACU}\end{matrix} - \begin{matrix}5'\text{CA}\\ 3'\text{GU}\end{matrix} - \begin{matrix}5'\text{AU}\\ 3'\text{UA}\end{matrix} - \begin{matrix}5'\text{UG}\\ 3'\text{AC}\end{matrix}\right) \quad (3b)$$

The two methods yielded $\Delta G^\circ_{\text{loop}}$ values differing by ~0.2 kcal/mol for both sets of duplex RNAs. Method 1 gave the slightly higher values. The average was used in Table 2.

Positive $\Delta G^\circ_{\text{loop}}$ increments were obtained for all tandem mismatches that were examined. The loop free energies ranged from 0.9 to 1.9 kcal/mol for the tandem mismatches with A·U and G·C closing base pairs, and from 1.5 to 1.8 kcal/mol for C·G and G·C closing base pairs. The three least stable tandem mismatches for both closing base pair environments were UC/AU, AU/UA, and AU/UC. Each of these sequences had a $\Delta G^\circ_{\text{loop}}$ of 1.8 or 1.9 kcal/mol for both closing base pair environments. The two most stable tandem mismatches were UU/UC and GU/UA, observed for the RNA molecules with A·U and G·C closing base pairs. Predicted $\Delta G^\circ_{\text{loop}}$ values (*4*) for the tandem mismatches are listed in Table 2. The GU/UA mismatch exhibited the largest discrepancy between predicted and measured values. If this tandem mismatch is excluded, the average difference between predicted and measured $\Delta G^\circ_{\text{loop}}$ values for the remaining 2 × 2 loops is 0.7 kcal/mol.

Estimated Heat Capacity Change for RNA Transitions. The average heat capacity change associated with RNA duplex denaturation, ΔC_p, was estimated from data on two RNA duplexes. Enthalpy and entropy changes were evaluated from melting curves obtained at concentrations from 1 to 75 μM and plotted as a function of T_m and ln T_m, respectively (*32*). Figure 5 shows plots of the ΔH and ΔS data for the GAUA/UUAC RNA duplex in a solvent with 100 mM Na^+. The slope of the linear regression line to the ΔH versus T_m data gives a value of 68 cal (mol of base pairs)$^{-1}$ K^{-1} ($R^2 = 0.83$). The entropy data produced a linear regression slope of 63 cal (mol of base pairs)$^{-1}$ K^{-1} with a similar R^2. Measurements were also made for the tandem mismatch RNA CauG/CuaG in the 1 M Na^+ solvent. Plots of ΔH and ΔS as a function of T_m and ln T_m yielded values of 74.3 and 74.6 cal (mol of base pairs)$^{-1}$ K^{-1}, respectively, with R^2 values of 0.70.

Assuming an average heat capacity change (ΔC_p) for all RNA duplexes of ≈70 cal (mol of base pairs)$^{-1}$ K^{-1}, the enthalpy and entropy changes evaluated in the transition region can be extrapolated to 37 °C using the equations

$$\Delta H(T_m) = \Delta H(T) + \Delta C_p(T_m - T) \quad (4a)$$

$$\Delta S(T_m) = \Delta S(T) + \Delta C_p \ln(T_m/T) \quad (4b)$$

Employing eq 4 decreases ΔH°_{37} and ΔS°_{37} for the two 10 bp RNA duplexes by ~16%, and decreases ΔH°_{37} and ΔS°_{37} for the tandem mismatch RNAs by only ~2.5%. Equation 4 has a negligible influence on ΔG°_{37} evaluated for the tandem mismatch RNAs, which have T_m's close to 37 °C; however, they decrease ΔG°_{37} for GAUA/UAUC by ~0.6 kcal/mol to −16.67 kcal/mol and decrease ΔG°_{37} of CAUG/CAUG by ~0.3 kcal/mol.

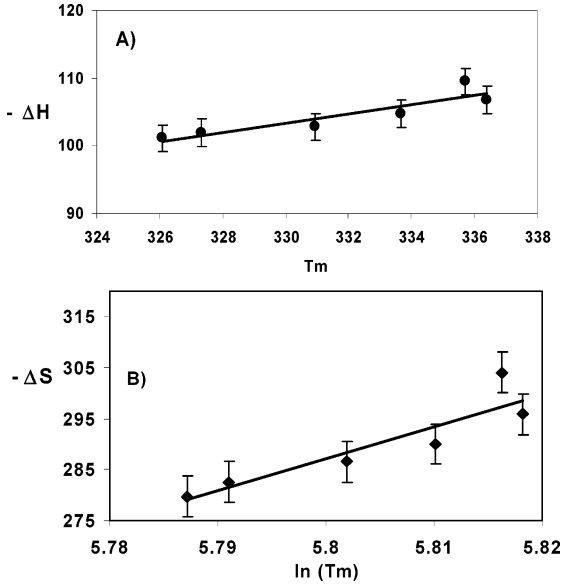

FIGURE 5: Plots of enthalpy change vs T_m and entropy change vs ln T_m evaluated from the melting curves of the GAUA/UUAC RNA duplex obtained at different strand concentrations in 100 mM Na^+.

From eq 3b, assuming the sum of stacking free energies is unaltered if one considers non-zero ΔC_p, the loop free energies would increase by ~ 0.6 kcal/mol for set 1 tandem mismatches and by ~0.3 kcal/mol for set 2 tandem mismatches. Thus, consideration of a heat capacity change may slightly increase the values of $\Delta G^\circ_{\text{loop}}$. The stacking free energies were evaluated assuming temperature-independent enthalpy and entropy changes (*16*). However, they were obtained using thermodynamic parameters averaged from melting curves with T_m values generally close to 37 °C. Thus, consideration of ΔC_p may not significantly alter these values.

DISCUSSION

Results from this study yielded destabilizing free energy increments for 16 tandem mismatches containing a single U-U mismatch adjacent to another noncanonical base pair. One mismatch GU/UA predicted to be stabilizing at 37 °C ($\Delta G^\circ_{\text{loop}} < 0$) gave free energy increments 1.7 or 2.0 kcal/mol higher than expected. $\Delta G^\circ_{\text{loop}}$ values for the 14 remaining sequences differed from predicted values by an average of 0.7 kcal/mol. This level of agreement is reasonably good given the idiosyncratic dependence of loop free energy on sequence that is sometimes observed (*28*).

The three tandem mismatches that were the least stable were the same for both closing base pair environments and gave similar loop free energies. The most stable tandem mismatches, GuuA/UucG and GauA/UuaC, were observed with G·C and A·U closing base pairs rather than the two closing G·C pairs. These results are not consistent with the notion that replacing a closing G·C base pair with an A·U pair increases $\Delta G^\circ_{\text{loop}}$ (*24*). Since relatively few measurements have been made on tandem mismatches with G·C and A·U closing base pairs, additional data on tandem mismatches and other internal loops in this environment are desirable.

The melting curve analysis employed in generating Tables 1 and 2 assumed temperature-independent enthalpy and entropy changes consistent with previous studies on RNA thermodynamic parameters. It also assumes that the thermodynamic parameters governing duplex nucleation are the same for perfectly matched and mismatched RNA duplexes. Inclusion of a non-zero heat capacity change can contribute significantly to $\Delta H°$ and $\Delta S°$ individually, but these two changes largely cancel each other when summed to give $\Delta G°$. This was observed when the thermodynamic parameters were adjusted for a heat capacity change using eq 4. $\Delta G°_{37}$ values for the 10 bp RNA duplexes changed by relatively small amounts, and a negligible effect was noted for the $\Delta G°_{37}$ values of the tandem mismatch RNAs. The average heat capacity change estimated in this study is in the range determined from previous analyses of other RNA oligomers [55−98 cal (mol of base pairs)$^{-1}$ K^{-1}] (*32*, *33*).

The self-complementary structures formed by some of the single-stranded oligonucleotides point out the need to consider single-strand states in analyzing the transitions of RNA duplexes. This was previously done in studies of RNA duplexes with asymmetric loops (*28*). Holbrook et al. (*37*) showed that the conformational equilibria of individual DNA single strands can contribute to the thermodynamics of duplex formation in several ways. The broad noncooperative transition between an ordered single strand and its totally unstructured state contributes to the temperature-dependent changes in the thermodynamic parameters governing duplex formation. Single strands that can form stable self-complementary duplexes or intramolecular hairpins may compete with the formation of non-self-complementary duplexes. Although the influence of self-complementary single-strand structures was small for most molecules that were examined, the coupled melting curve analysis was required for several RNA duplex transitions.

An algorithm recently developed by Zuker and colleagues (*38*, *39*) describes a partition function approach to predicting heteroduplex melting curves that includes the effects of individual strands forming self-complementary duplexes. The algorithm predicted the coupled transitions for the heteroduplexes involving strand 2BUC. The predicted curves did not exhibit the two transition steps observed but clearly illustrated the influence of the self-complementary duplex transitions. Transition T_m's predicted for the fully base paired duplexes GAUA/UAUC and CAUG/CAUG were 5.4 and 2.4 °C below our experimental values, respectively. These differences likely reflect the parameters employed by the algorithm.

The 2BUC single strand can be written as a self-complementary duplex with six consecutive Watson−Crick base pairs and G-G terminal mismatches on both ends.

5' UCGCUCGAGG 3'
• • • • • •
3' GGAGCUCGCU 5'

Calculating $\Delta H°$ and $\Delta S°$ values for this structure at 1 M Na^+ from nearest neighbor parameters (*15*, *16*), one predicts a T_m of 47.8 °C for a C_t of 4.8 μM from the equation $T_m = \Delta H°/(R \ln C_t + \Delta S°)$. This value is in excellent agreement with experiment and supports the proposed structure.

APPENDIX

Coupled Melting Transitions of a Nucleic Acid Duplex with a Competing Single-Strand Self-Complementary Duplex. We consider the denaturation of a nucleic acid duplex comprised of two complementary strands S1 and S2, when one of the strands (strand S1) is able to form a partial self-complementary duplex. Extending this analysis to a situation where both strands can form self-complementary duplexes is described below. For the case considered, there are four possible molecular states: D12, the duplex formed from S1 and S2; D11, the duplex formed by two S1 strands; and the two single strands.

The absorbance versus temperature curve is given by

$$A(T) = c_{12}\epsilon_{12} + c_{11}\epsilon_{11} + c_1\epsilon_1 + c_2\epsilon_2 \quad (5)$$

c_{12} and c_{11} are the concentrations of the D12 and D11 duplexes, respectively (moles of duplex per liter). They are dependent on temperature T. Similarly, c_1 and c_2 are the concentrations of strands S1 and S2, respectively (moles of strand per liter). The extinction coefficients, ϵ_{ij} and ϵ_i, may also be considered temperature-dependent, reflecting changes in the duplex and single-stranded states. The total concentrations of strands S1 and S2 are the same ($c_{T1} = c_{T2} = c_T/2$). Mass conservation yields the equations

$$c_{T1} = c_{12} + 2c_{11} + c_1 \quad (6a)$$

$$c_{T2} = c_{12} + c_2 \quad (6b)$$

The fraction of total strand S2 that is a D12 duplex is given by $\theta_{12} = 2c_{12}/c_T$, and the fraction of total strand S1 that is a D11 duplex is given by $\theta_{11} = 4c_{11}/c_T$.

From eqs 5 and 6 and the definitions of θ_{12} and θ_{11}, one can rewrite $A(T)$ as

$$A(T) = c_T/2[\theta_{12}\epsilon_{12} + \theta_{11}\epsilon_{11}/2 + (1 - \theta_{12} - \theta_{11})\epsilon_1 + (1 - \theta_{12})\epsilon_2] \quad (7)$$

The experimental melting transition normalized between 0 and 1 is obtained from the equation

$$\phi(T) = [A(T) - A^d(T)]/[A^s(T) - A^d(T)] \quad (8)$$

where $A^d(T)$ is the low-temperature linear baseline absorbance corresponding to the duplex state and $A^s(T)$ is the high-temperature baseline corresponding to the single-stranded states of the two strands. From eq 5, the latter may also be expressed as

$$A^s(T) = c_T/2(\epsilon_1 + \epsilon_2) \quad (9)$$

From eqs 7−9, one can rewrite $\phi(T)$ as

$$\phi(T) = 1 + \frac{(\epsilon_{12} - \epsilon_1 - \epsilon_2)\theta_{12}}{B} + \frac{(\epsilon_{11}/2 - \epsilon_1)\theta_{11}}{B} \quad (10)$$

where $B = 2[A^s(T) - A^d(T)]/c_T$. B is measured experimentally from the melting transitions. The extinction coefficients ϵ_1 and ϵ_2 and their temperature dependence were estimated from the high-temperature absorbance profile of individual strands. ϵ_{12} was estimated from the linear baseline absorbance

between 5 and 10 °C and strand concentration. It was assumed that an equimolar mixture of strands S1 and S2 is fully duplexed in the D12 state in this temperature range. ϵ_{11} was estimated in a similar way under conditions where only strand S1 is present and the self-complementary duplex transition begins above 10 °C. For the three RNA duplexes involving the 2BUC oligonucleotide, the coefficient of θ_{12} in eq 10 varied between −0.97 and −1.02 and the coefficient of θ_{11} ranged from −0.40 to −0.45. Values of −1 and −0.42 were employed.

Coupled equations of θ_{12} and θ_{11} were expressed in terms of the equilibrium constants describing the formation of the self-complementary and non-self-complementary duplexes, and relevant concentrations. The two coupled reactions are described as

$$2S1 \overset{K_{11}}{\rightleftharpoons} D11 \text{ and } S1 + S2 \overset{K_{12}}{\rightleftharpoons} D12 \quad (11)$$

From the definition of θ_{12}, the relation of association equilibrium constants to concentrations from eq 11, and eq 6, one can express θ_{12} as

$$\theta_{12} = K_{12}c_{T2}(1 - \theta_{12})/[K_{12}c_{T2}(1 - \theta_{12}) + 2K_{11}\theta_{12}/K_{12}\theta_{11}] \quad (12)$$

Similarly, one can write θ_{11} as a function of θ_{12}

$$\theta_{11} = (1 - \theta_{12})(2K_{11}/K_{12})\theta_{12}/[(2K_{11}/K_{12})\theta_{12} + (1 - \theta_{12})] \quad (13)$$

Values of $K_{11}(T)$ are obtained from $\Delta H_{11}°$ and $\Delta S_{11}°$ evaluated from the melting curve of the D11 duplex and the relation of the equilibrium constant and standard free energy change.

$$K(T) = \exp[-(\Delta H° - T\Delta S°)/RT] \quad (14)$$

Estimated values of $\Delta H_{12}°$ and T_{m12} were used to generate trial values of $K_{12}(T)$ using the integral form of the van't Hoff equation

$$K_{12}(T) = (4/c_T)\exp[(\Delta H_{12}°/R)(1/T_{m12} - 1/T)] \quad (15)$$

θ_{12} and θ_{11} are numerically solved from eqs 12 and 13 at temperatures spanning the melting curve. The two fractions were then used in eq 10 to calculate normalized melting curves that were compared with experiment.

The analysis described above can be extended to situations where both single strands can form stable self-complementary duplexes. A similar numerical approach is employed. In this case, θ_{12} was related to θ_1 and θ_2, where θ_1 is the fraction of strand S1 in its single-stranded state and θ_2 is the fraction of strand S2 in its single-stranded state. From the three fractions and an equation describing strand conservation, one calculates θ_{11} and θ_{22}. The three coupled equations are

$$\theta_{12} = K_{12}c_{T1}\theta_1\theta_2/[K_{12}c_{T1}\theta_1\theta_2 + (1 - \theta_{12})] \quad (16a)$$

$$\theta_1 = \{-1 + [1 + 8K_{11}c_{T1}(1 - \theta_{12})]^{1/2}\}/4K_{11}c_{T1} \quad (16b)$$

$$\theta_2 = \{-1 + [1 + 8K_{22}c_{T2}(1 - \theta_{12})]^{1/2}\}/4K_{22}c_{T2} \quad (16c)$$

SUPPORTING INFORMATION AVAILABLE

Thermodynamic data from melting curves of single-stranded oligonucleotides. This material is available free of charge via the Internet at http://pubs.acs.org.

REFERENCES

1. Mathews, D. H., Sabina, J., Zuker, M., and Turner, D. H. (1999) Expanded sequence dependence of thermodynamic parameters improves prediction of RNA secondary structure, *J. Mol. Biol. 288*, 911−40.
2. Rivas, E., and Eddy, S. R. (1999) A dynamic programming algorithm for RNA structure prediction including pseudoknots, *J. Mol. Biol. 285*, 2053−68.
3. Zuker, M. (2003) Mfold web server for nucleic acid folding and hybridization prediction, *Nucleic Acids Res. 31*, 3406−15.
4. Mathews, D. H., Disney, M. D., Childs, J. L., Schroeder, S. J., Zuker, M., and Turner, D. H. (2004) Incorporating chemical modification constraints into a dynamic programming algorithm for prediction of RNA secondary structure, *Proc. Natl. Acad. Sci. U.S.A. 101*, 7287−92.
5. Ding, Y., and Lawrence, C. E. (2003) A statistical sampling algorithm for RNA secondary structure prediction, *Nucleic Acids Res. 31*, 7280−301.
6. de Smit, M. H., and van Duin, J. (1994) Control of translation by mRNA secondary structure in *Escherichia coli*. A quantitative analysis of literature data, *J. Mol. Biol. 244*, 144−50.
7. de Smit, M. H., and van Duin, J. (2003) Translational standby sites: How ribosomes may deal with the rapid folding kinetics of mRNA, *J. Mol. Biol. 331*, 737−43.
8. Mahen, E. M., Harger, J. W., Calderon, E. M., and Fedor, M. J. (2005) Kinetics and thermodynamics make different contributions to RNA folding in vitro and in yeast, *Mol. Cell 19*, 27−37.
9. Lease, R. A., and Woodson, S. A. (2004) Cycling of the Sm-like protein Hfq on the DsrA small regulatory RNA, *J. Mol. Biol. 344*, 1211−23.
10. Wu, M., and Tinoco, I., Jr. (1998) RNA folding causes secondary structure rearrangement, *Proc. Natl. Acad. Sci. U.S.A. 95*, 11555−60.
11. Brescia, C. C., Mikulecky, P. J., Feig, A. L., and Sledjeski, D. D. (2003) Identification of the Hfq-binding site on DsrA RNA: Hfq binds without altering DsrA secondary structure, *RNA 9*, 33−43.
12. Ruschak, A. M., Mathews, D. H., Bibillo, A., Spinelli, S. L., Childs, J. L., Eickbush, T. H., and Turner, D. H. (2004) Secondary structure models of the 3′ untranslated regions of diverse R2 RNAs, *RNA 10*, 978−87.
13. Pappalardo, L., Kerwood, D. J., Pelczer, I., and Borer, P. N. (1998) Three-dimensional folding of an RNA hairpin required for packaging HIV-1, *J. Mol. Biol. 282*, 801−18.
14. Diamond, J. M., Turner, D. H., and Mathews, D. H. (2001) Thermodynamics of three-way multibranch loops in RNA, *Biochemistry 40*, 6971−81.
15. Serra, M. J., and Turner, D. H. (1995) Predicting thermodynamic properties of RNA, *Methods Enzymol. 259*, 242−61.
16. Xia, T., SantaLucia, J., Jr., Burkard, M. E., Kierzek, R., Schroeder, S. J., Jiao, X., Cox, C., and Turner, D. H. (1998) Thermodynamic parameters for an expanded nearest-neighbor model for formation of RNA duplexes with Watson−Crick base pairs, *Biochemistry 37*, 14719−35.
17. Zhu, J., and Wartell, R. M. (1999) The effect of base sequence on the stability of RNA and DNA single base bulges, *Biochemistry 38*, 15986−93.
18. Znosko, B. M., Silvestri, S. B., Volkman, H., Boswell, B., and Serra, M. J. (2002) Thermodynamic parameters for an expanded nearest-neighbor model for the formation of RNA duplexes with single nucleotide bulges, *Biochemistry 41*, 10406−17.
19. Xia, T., McDowell, J. A., and Turner, D. H. (1997) Thermodynamics of nonsymmetric tandem mismatches adjacent to G·C base pairs in RNA, *Biochemistry 36*, 12486−97.
20. Kierzek, R., Burkard, M. E., and Turner, D. H. (1999) Thermodynamics of single mismatches in RNA duplexes, *Biochemistry 38*, 14214−23.
21. Zhu, J., and Wartell, R. M. (1997) The relative stabilities of base pair stacking interactions and single mismatches in long RNA measured by temperature gradient gel electrophoresis, *Biochemistry 36*, 15326−35.

22. Serra, M. J., Barnes, T. W., Betschart, K., Gutierrez, M. J., Sprouse, K. J., Riley, C. K., Stewart, L., and Temel, R. E. (1997) Improved parameters for the prediction of RNA hairpin stability, *Biochemistry 36*, 4844−51.
23. Serra, M. J., Lyttle, M. H., Axenson, T. J., Schadt, C. A., and Turner, D. H. (1993) RNA hairpin loop stability depends on closing base pair, *Nucleic Acids Res. 21*, 3845−9.
24. Burkard, M. E., Xia, T., and Turner, D. H. (2001) Thermodynamics of RNA internal loops with a guanosine-guanosine pair adjacent to another noncanonical pair, *Biochemistry 40*, 2478−83.
25. Wu, M., McDowell, J. A., and Turner, D. H. (1995) A periodic table of symmetric tandem mismatches in RNA, *Biochemistry 34*, 3204−11.
26. McDowell, J. A., and Turner, D. H. (1996) Investigation of the structural basis for thermodynamic stabilities of tandem GU mismatches: Solution structure of $(rGAGGUCUC)_2$ by two-dimensional NMR and simulated annealing, *Biochemistry 35*, 14077−89.
27. Chen, G., Znosko, B. M., Jiao, X., and Turner, D. H. (2004) Factors affecting thermodynamic stabilities of RNA 3×3 internal loops, *Biochemistry 43*, 12865−76.
28. Schroeder, S. J., and Turner, D. H. (2000) Factors affecting the thermodynamic stability of small asymmetric internal loops in RNA, *Biochemistry 39*, 9257−74.
29. Schroeder, S. J., and Turner, D. H. (2001) Thermodynamic stabilities of internal loops with GU closing pairs in RNA, *Biochemistry 40*, 11509−17.
30. Schroeder, S., Kim, J., and Turner, D. H. (1996) G·A and U·U mismatches can stabilize RNA internal loops of three nucleotides, *Biochemistry 35*, 16105−9.
31. SantaLucia, J., Jr., Kierzek, R., and Turner, D. H. (1991) Stabilities of consecutive A·C, C·C, G·G, U·C, and U·U mismatches in RNA internal loops: Evidence for stable hydrogen-bonded U·U and C·C·+ pairs, *Biochemistry 30*, 8242−51.
32. Rouzina, I., and Bloomfield, V. A. (1999) Heat capacity effects on the melting of DNA. 1. General aspects, *Biophys. J. 77*, 3242−51.
33. Petersheim, M., and Turner, D. H. (1983) Base-stacking and base-pairing contributions to helix stability: Thermodynamics of double-helix formation with CCGG, CCGGp, CCGGAp, ACCGGp, CCGGUp, and ACCGGUp, *Biochemistry 22*, 256−63.
34. Gray, D. M., Hung, S. H., and Johnson, K. H. (1995) Absorption and circular dichroism spectroscopy of nucleic acid duplexes and triplexes, *Methods Enzymol. 246*, 19−34.
35. Cavaluzzi, M. J., and Borer, P. N. (2004) Revised UV extinction coefficients for nucleoside-5′-monophosphates and unpaired DNA and RNA, *Nucleic Acids Res. 32*, e13.
36. Marky, L. A., and Breslauer, K. J. (1987) Calculating thermodynamic data for transitions of any molecularity from equilibrium melting curves, *Biopolymers 26*, 1601−20.
37. Holbrook, J. A., Capp, M. W., Saecker, R. M., and Record, M. T., Jr. (1999) Enthalpy and heat capacity changes for formation of an oligomeric DNA duplex: Interpretation in terms of coupled processes of formation and association of single-stranded helices, *Biochemistry 38*, 8409−22.
38. Dimitrov, R. A., and Zuker, M. (2004) Prediction of hybridization and melting for double-stranded nucleic acids, *Biophys. J. 87*, 215−26.
39. Markham, N. R., and Zuker, M. (2005) DINAMelt web server for nucleic acid melting prediction, *Nucleic Acids Res. 33*, W577−81.

BI051659Q